Field measurement and model prediction of rail corrugation

Chen G X [1],*, Zhang S[1], Wu B W [1], Zhao X N [1], Wen Z F [1], Ouyang H[2], Zhu M H[1]

[1] The State Key Laboratory of Traction Power, Southwest Jiaotong University, Chengdu, China

[2] School of Engineering, University of Liverpool, the Quadrangle, Liverpool L69 3GH, UK

Abstract: In a field test, three corrugation profiles of rails and their corresponding vibrations were measured, and the wavelengths and frequencies of rail corrugations obtained. In the model prediction, finite-element models of the self-excited vibrations corresponding to three different wheelset-track systems were established. The corrugation frequencies of these models were predicted, and a comparison between the measured and predicted corrugation frequencies shows that they are in good agreement. It can be concluded that self-excited vibration of a wheelset-track system can cause rail corrugation. A benchmark condition for the validation of rail corrugation models is proposed.

1. Introduction

Nowadays, rail corrugation has been seldom reported in Chinese main-line railway tracks. It may be attributed to the application of worn-type tread profiles and the adoption of the minimum curved track radius of 500–600 m. However, rail corrugation is still an elusive problem in metro tracks all over the world. Almost all low rails on tight curved tracks, the radii of which are less than 350 m in China, suffer from rail corrugation. The length of corrugated rails occurring on the low rails of tight curved tracks makes up more than 80% of the total length of all corrugated rails. In the early 1900s, railway administrators and researchers paid attention to rail corrugation. Over the years, many experimental and theoretical studies have led to good understanding of the generation mechanism for rail corrugation [1–4]. It is generally accepted that rail corrugation depends on the wavelength-fixing and material-removal mechanisms [1]. Now, the most widely accepted prediction model of rail corrugation is based on the wheel–rail interaction due to rail surface roughness. In the model, the rail surface roughness causes vibration of the wheel–rail system, which leads to a fluctuation of the friction power of the wheel–rail contact interface. According to the known fact that the fluctuation of the friction power leads to undulant wear, the rail work surface subsequently suffers from corrugation [5–15]. Stick-slip motion of wheel-rail systems as a possible mechanism for rail corrugation was also studied [16–19]. Experimental studies have accumulated a significant amount of information on the nature of rail corrugation and have validated several prediction models [20–25]. Up to now, great achievements have been made in the field of rail corrugation. Rail corrugation can be supressed largely by grinding, friction modifiers, and variation of passage speed.

The only negative aspects regarding rail corrugation, currently, are that the occurrence probability of rail corrugation on the low rail of tight curved tracks is still close to 100% and the practical remedies for rail corrugation are passive. In the research field of rail corrugation, there is a very common and deterministic phenomenon of rail corrugation (the CD phenomenon of rail corrugation), namely almost all low rails on tight curved tracks the radii of which are less than 350 m in China suffer from rail corrugation, but high rails on the same curved track rarely suffer from rail corrugation. The rails on smooth curved tracks the radii of which are larger than 650–800 m or on straight tracks rarely suffer from rail corrugation. The relevant literature does not indicate why almost all low rails on tight curved tracks suffer from rail

corrugation but high rails on the same curved track rarely suffer from rail corrugation. It is also unknown why the rails on smooth curved tracks or on straight tracks rarely and uncertainly suffer from rail corrugation. We believe this is attributed to a lack of understanding of some generation mechanisms of rail corrugation. Because of these flaws in existing rail corrugation theories, several researchers have proposed improved rail corrugation models to better understand the generation mechanism for rail corrugation. Among these improved models, Vila *et al*. [26] studied the evolution of rail corrugation using a rotating flexible wheelset model and concluded that the dynamics of the rotating flexible wheelset might give rise to generation mechanisms of rail corrugation. Baeza *et al*. [27] studied prediction of rail corrugation using a rotating flexible wheelset coupled with a flexible track model and a non-Hertzian/non-steady contact model, and found that the third bending mode of the rotating flexible wheelset causes significant contact forces and that the wear depths estimated using the rotating flexible wheelset are much higher than those predicted by using the rigid wheelset model and the frequency of wear is twice the corrugation frequency. Jin *et al*. [28] established a comprehensive rail corrugation model including a bogie and a car body, in which Kalker's non-Hertzian wheel–rail contact was taken into account, and concluded that the track stiffness has a great influence on the initiation and development of rail corrugation. Bellette *et al*. [29] studied the influence of contact-induced wear filtering and its influence on corrugation growth and concluded that the contact filtering effect only significantly amplifies short-pitch corrugation growth when corrugation amplitudes are small (order of 1 μm). Over multiple vehicle passes, this contact-amplifying effect is shown to decrease to a negligible level and the peak amplitude shifts to longer wavelengths. Alternatively, Chen, one of the authors of this study, and other co-authors proposed the friction-induced self-excited vibration of a wheelset–track system as a possible wavelength-fixing mechanism for rail corrugation in 2010 [30]. Later, Chen and his colleagues carried out further work and found that their model could succeed in reproducing most rail corrugation phenomena, including the above-mentioned CD phenomenon of rail corrugation [31,32]. Omar [33] applied a similar method to study rail corrugation in his Master's dissertation.

Several reviewers have expressed their concerns about the validation of the authors' models in reviewing the authors' manuscripts on the friction-induced self-excited vibration of a wheelset-track system as a possible mechanism for rail corrugation. In the authors' viewpoint, the friction-induced self-excited vibration of a wheelset–track system belongs to the category of the stick-slip motion. It is generally accepted that the stick-slip motion of a wheel-rail system is a possible mechanism for rail corrugation. Unfortunately, to our best knowledge, there are a very few studies that deal with the validation of the stick-slip motion causing rail corrugation in the literature. The authors spent two to three years reflecting on the validation of the authors' model, and this study presents our work on the validation of the authors' model. Before introducing our work, it is necessary to review the the validation of rail corrugation models.

In the literature, the validation method generally comprises the following procedures [20,21,25,34]: (1) Measure a profile of the rail working surface without rail corrugation along the longitudinal direction of the rail, (2) measure several different profiles of the rail working surface with rail corrugation along the longitudinal direction of the rail to obtain the evolution of rail corrugation with time, (3) establish a rail corrugation model and perform a numerical analysis of the model to obtain the evolution of rail corrugation with time, and (4) compare the measured and numerical results of rail corrugation and draw a conclusion. Several researchers have reported successfully validating their models [20,21,25,34].

Our aim of this work was to present a comparison study between the field measurement and predicted results. The existing validation methods of rail corrugation models are discussed and a benchmark condition for the validation of rail corrugation models proposed.

2. Field test measurements

In Beijing metro line 4, the designers used five types of sleepers or track structures to suppress vibration and noise due to the wheel−rail interaction, which include a short sleeper, a booted short sleeper, a Cologne-egg damping fastener, a ladder sleeper track, and a floating slab track. Contrary to expectation, however, the vibration and noise become worse in some track sections. Further field investigations showed that the strong vibration and noise are due to rail corrugation. To better understand the generation mechanism for rail corrugation, the authors made field measurements of rail corrugation profiles, track parameters, and rail vibration when metro trains passed through.

2.1 Rail corrugation profile measurements

The total length of Beijing metro line 4 is approximately 28 km. All low rails of tight curved tracks the radii of which are less than or equal to 350 m are subjected to corrugation. Some low rails of a tight curved track of radius 450 m are also subjected to corrugation. Two rails of some tangential tracks equipped with Cologne-egg damping fasteners are also subjected to corrugation. A Danish ODS wheel and rail roughness measuring system was used to measure rail corrugation profiles, as shown in Figure 1.

Figure 1 Photograph of ODS wheel and rail roughness measuring system.

2.2 Rail vibration measurements

In Beijing metro line 4, three test sites were chosen to measure rail corrugations and rail vibrations. Accelerometers were used to measure vibrations of rails and sleepers. The vertical and lateral vibrations of the rail points at the central positions between two sleepers and above a sleeper, and the vertical vibration of the sleeper, were measured simultaneously. Figure 2 shows the positions of the accelerometers on rails and sleepers at the three test sites. The track layouts and fastener types of these three test sites are listed in Table 1.

Table 1 Track layouts and fastener types of test sites.

Test site	Track layout	Fastener type
1	Curved track of radius 350 m	DTVI2
2	Tangential track	Cologne-egg
3	Curved track of radius 350 m	DTIII2

(a)

(b)

(c)

(d)

Figure 2 *Positions of accelerometers: (a) low rail at test site 1, (b) left rail at test site 2, (c) right rail at test site 2, and (d) low rail at test site 3.*

2.3 Fastener stiffness and damping measurements

Fastener stiffness and damping were measured by the authors' colleagues in the laboratory. The measurement data are presented as follows:

(1) DTVI2-type fastener: the vertical stiffness of the fastener is k_v=40.73 kN/mm, the vertical damping coefficient of the fastener is c_v=9898.70 Ns/m, the lateral stiffness of the fastener is k_l=8.79 kN/mm, and the lateral damping coefficient of the fastener is c_l=1927.96 Ns/m.

(2) Cologne-egg damping fastener: k_v=12.07 kN/mm, c_v=1361.12 Ns/m, k_l=7.58 kN/mm, and c_l=974.27 Ns/m.

(3) DTIII2-type fastener: k_v=18.28 kN/mm, c_v=6361.29 Ns/m, k_l=9.00 kN/mm, and c_l=1830.22Ns/m.

3. Rail corrugation modeling

Combining the knowledge of friction-induced vibration and of vehicle system dynamics, Chen and co-authors proposed the friction-induced self-excited vibration of a wheelset-track system as a possible wavelength-fixing mechanism for rail corrugation [30]. In a tight curved track, the creep force between the wheel and rail is approximately equal to the friction force; that is, the normal force times the coefficient of friction. The motion equation of the wheelset-track system can be written as follows [30]:

$$\mathbf{M_r}\ddot{u}+\mathbf{C_r}\dot{u}+\mathbf{K_r}u=0, \qquad (1)$$

where u is the displacement vector of nodes. Each node has three displacement components, u_1, u_2, and u_3, which are the displacement components in the x-axis direction, y-axis direction, and z-axis direction, respectively. $\mathbf{M_r}$, $\mathbf{C_r}$, and $\mathbf{K_r}$ are the mass, damping, and stiffness matrices, respectively, and are asymmetric matrices due to friction. The eigenvalue equation of Eq. (1) is presented in the following form:

$$(\mathbf{M_r}\lambda^2 + \mathbf{C_r}\lambda + \mathbf{K_r})\phi=0, \qquad (2)$$

where λ is an eigenvalue. The general solution of Eq (1) is written as follows:

$$u(t) = \sum \phi_i \exp(\lambda_i t) = \sum \phi_i \exp((\alpha_i + j\omega_i)t), \qquad (3)$$

where ϕ_i is the ith eigenvector of Eq. (2) and $\lambda_i = \alpha_i + j\omega_i$ the ith eigenvalue of Eq (2), α_i and ω_i the real and imaginary parts of the ith eigenvalue, respectively, and j is an imaginary unit. From Eq. (3), it is seen that when a real part of the eigenvalues is larger than zero the displacement will increase with time; that is, the vibration of the system becomes unstable.

Figures 3−5(a) show finite-element models of three metro wheelset-track systems, which correspond to those wheelset-track systems in test sites 1–3 shown in Figure 2, respectively. Figure 5(b) shows a picture of a ladder track, which is presented to illustrate the construction of a ladder track for readers. The main parameters of models 1–3 are listed in Table 2. Model 1 consists of two wheels, an axle, two rails, a series of short sleepers, and railpads. There are 403907 nodes and 282324 C3D8I elements in model 1. The model has been improved in the following two details: the wheelset and railpad. In the present model, two wheels and an axle were assembled into a wheelset by interference fits. In the authors' previous models [30], the wheelset was a single solid; that is, two wheels and an axle were cast into a single solid. In the present model, railpads were simulated with solid elements. In the authors' previous models [30], the railpad was simulated with massless and sizeless springs and dampers. According to Oregui et al. [35], using solid elements in place of massless and sizeless springs and dampers to simulate the railpad can obtain more realistic dynamic performances of the wheelset-track system. Model 2 consists of eight wheels, four axles, and two rails. There are 442942 nodes and 349288 C3D8I elements in model 2. The Cologne-egg fasteners were simulated with massless and sizeless springs and dampers. Model 3 consists of two wheels, an axle, two rails, several ladder sleepers, and railpads. There are 456300 nodes and 367782 C3D8I elements in model 3. In the model, two wheels and an axle were assembled into a wheelset by interference fits, and railpads were simulated with solid elements. In models 1 and 3, the friction-velocity slope was taken

into account. It was assumed that the coefficient of friction between the wheel and rail varies against the relative sliding speed according to the following formula [19]:

$$u_\mathrm{d} = 0.28 + (0.8 - 0.28)e^{-0.011V_r}, \tag{4}$$

where u_d is the kinetic coefficient of friction and V_r the relative sliding speed between the wheel and rail.

It should be mentioned that the modeling procedure for the corrugation prediction established by the authors is stationary, which was based mainly on the finite-element method. The involvement of researchers in this procedure is restricted to be low. The source code of the authors' prediction model is open to the public. Chen, one of the authors, also provided the ABAQUS source code of a prediction model for an engineer working on PERMAS, a finite-element package developed by INTES Engineering Software in Europe. The engineer transferred the ABAQUS source code into the PERMAS source code. His comparative analysis showed good agreement between the calculation results from ABAQUS and those from PERMAS.

Table 2 Main parameters of models 1–3.

Track	
Density of rail (kg/m^3)	7800
Young's modulus of rail (N/m^2)	2.1×10^{11}
Poisson's ratio of rail	0.3
Length of rail (m)	36
Type of rail (kg/m)	60
Sleeper spacing (m)	0.625
Rail cant	1/40
Density of railpad (kg/m^3)	1300
Young's modulus of railpad (N/m^2)	8.0×10^7
Poisson's ratio	0.45
Thickness of railpad (m)	0.012
Density of sleeper (kg/m^3)	2480
Young's modulus of sleeper (N/m^2)	1.9×10^{11}
Poisson's ratio of sleeper	0.3
Vertical support stiffness from monolithic track-bed (N/m)	8.9×10^7
Vertical support damping from monolithic track-bed (Ns/m)	8.98×10^4
Lateral support stiffness from monolithic track-bed (N/m)	5.0×10^7
Lateral support damping from monolithic track-bed (Ns/m)	4.0×10^4
Vehicle	
Gauge (mm)	1435
Wheelbase of bogie (mm)	2300
Profile of tread	LM-type worn profile
Mass of wheelset (kg)	1365
Moment of inertia of wheelset in vertical and lateral axes (kg m^2)	880
Moment of inertia of wheelset in rolling axis (kg m^2)	116
Mass of bogie (kg)	2028
Moment of inertia of bogie in longitudinal level axes (kg m^2)	983
Moment of inertia of bogie in lateral level axes (kg m^2)	582
Moment of inertia of bogie in vertical axes (kg m^2)	1506
Mass of car body (kg)	35030
Moment of inertia of car body in longitudinal level axes (kg m^2)	50370
Moment of inertia of car body in the lateral level axes (kg m^2)	1395430
Moment of inertia of car body in vertical axes (kg m^2)	1386060

Longitudinal stiffness of primary suspension alone (kN/m)	4850
Lateral stiffness of primary suspension alone (kN/m)	3430
Vertical stiffness of primary suspension alone (kN/m)	740
Vertical damping of primary suspension alone (kNs/m)	15.626
Vertical stiffness of secondary suspension alone (kN/m)	480
Lateral stiffness of secondary suspension alone (kN/m)	210
Vertical damping of secondary suspension alone (kNs/m)	50
Axle load (from Simpack simulation)	
Vertical load acting on an axlebox on tangential track (N)	47880
Lateral force acting on an axlebox on tangential track (N)	0
Vertical load acting on outer axlebox on curved track (N)	49800
Vertical load acting on inner axlebox on curved track (N)	45900
Lateral load acting on outer axlebox on curved track (N)	17100
Lateral load acting on inner axlebox on curved track (N)	13800

(a)

(b)
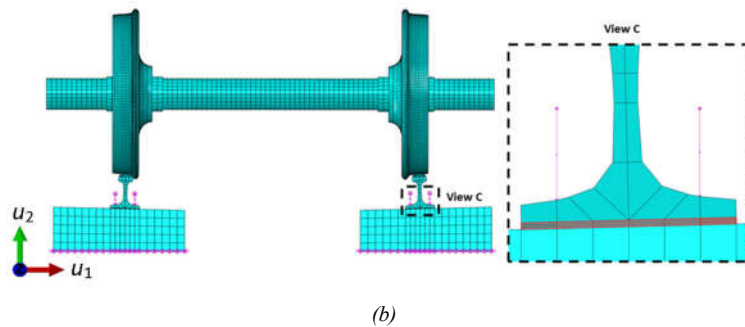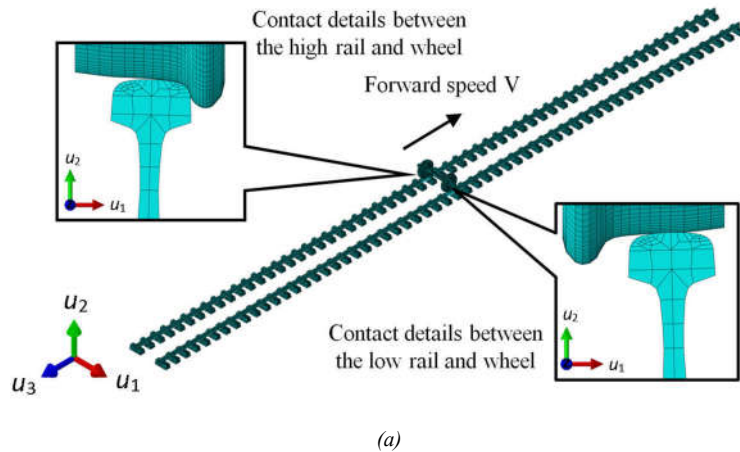
Figure 3 *Model 1 representing wheelset-track with short sleepers at test site 1: (a) overall view of model and (b) model details.*
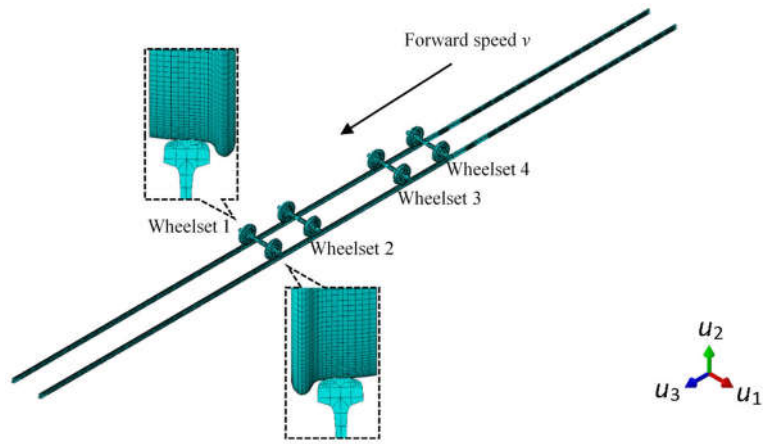
Figure 4 *Model 2 representing wheelset-track system at test site 2.*
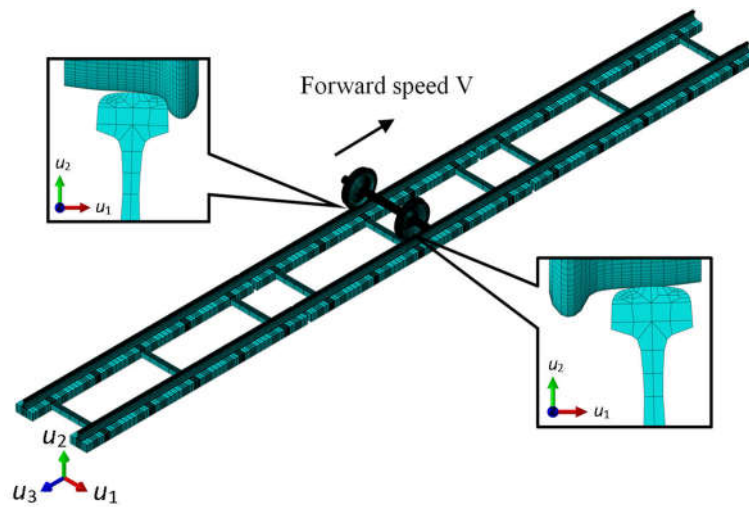
(a)

(b)

Figure 5 *Model 3 representing the wheelset-track system at test site 3: (a) finite-element model of ladder track-wheelset system and (b) photograph of ladder track.*

4. Results
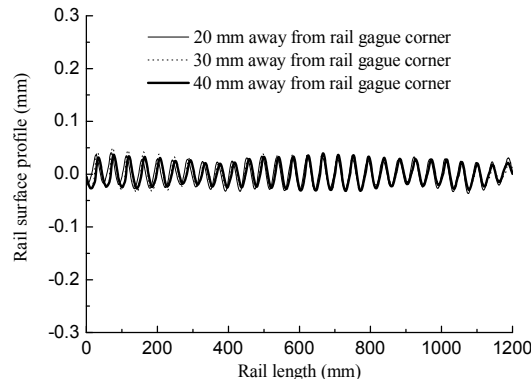
4.1 Rail corrugation profile measurement results

Figure 6 shows measurement results of rail surface profiles. Figure 6(a) shows the rail corrugation measurement result of the low rail at test site 1. Since the corrugation on the high rail is invisible to the eye, the rail corrugation measurement result of the high rail is not presented. From Figure 6(a), it is seen that the low rail is subjected to a clear corrugation with an amplitude of 0.236 mm at test site 1. The main wavelength of the low-rail corrugation is approximately 125 mm based on the 1/3-octave wavelength analysis. Figures 6(b) and 6(c) show the rail corrugation measurement results of the left and right rails at test site 2. From Figures 6(b) and 6(c), it is found that the left and right rails of the tangential track are subjected to severe corrugations, the amplitudes of which are approximately 0.05 mm. The main wavelength of rail corrugation is approximately 40 mm based on the 1/3-octave wavelength analysis. Figure 6(d) shows the rail corrugation measurement result of the low rail at test site 3. Since the corrugation on the high rail is invisible to the eye, the rail corrugation measurement result of the high rail is not presented. From Figure 6(d), it is seen that the low rail is subjected to an obvious corrugation with an amplitude of 0.124 mm. The main wavelength of rail corrugation is approximately 100 mm based on the 1/3-octave wavelength analysis.
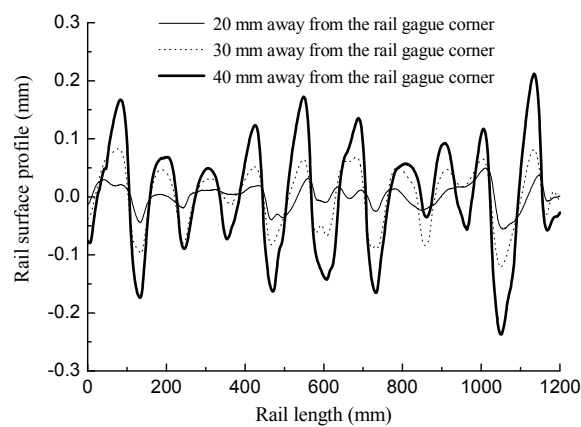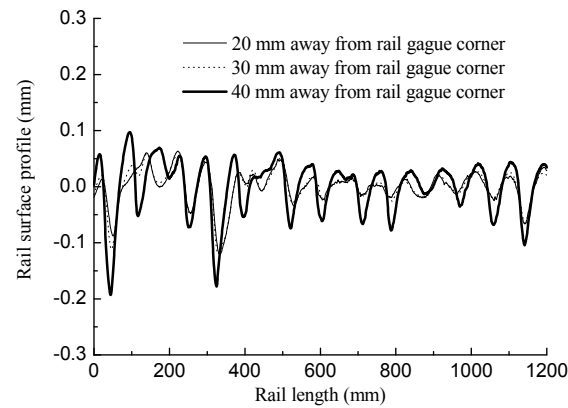

(a)
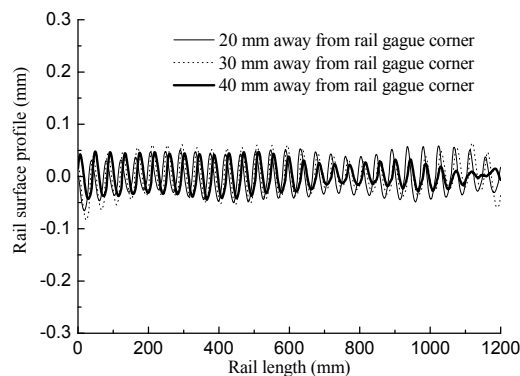

(b)

(c)

(d)

Figure 6 *Measurement results of rail surface profiles: (a) Low rail at test site 1, 13 months elapsed since previous rail grinding and 1200000 wheelset passage; (b) left rail at test site 2, 2.8 months elapsed since previous rail grinding and 260000 wheelset passage; (c) right rail at test site 2, 2.8 months elapsed since previous rail grinding and 260000 wheelset passage; (d) low rail at test site 3, 13 months elapsed since previous rail grinding and 260000 wheelset passage.*

4.2. Rail vibration measurement results

Rail vibration contains the frequency message of rail vibration, which corresponds to the frequency of rail corrugation. Figure 7 shows the rail vibrations measurement results when metro trains passed through the test sites. From Figure 7, it is seen that the vertical vibrations of rails in the presence of rail corrugation arrive at 200–600 m/s^2 in amplitude. Figure 8 shows a power-spectrum-density (PSD) analysis of these vibrations. From Figure 8(a), it is found that the main frequency of the rail vibration at test site 1 is approximately 80 Hz. From Figure 8(b) and (c), it is seen that the main frequency of the vibrations of the left and right rails at test site 2 is all approximately 320 Hz. From Figure 8(d), it is found that the main frequency of the rail vibration at test site 3 is approximately 134 Hz.
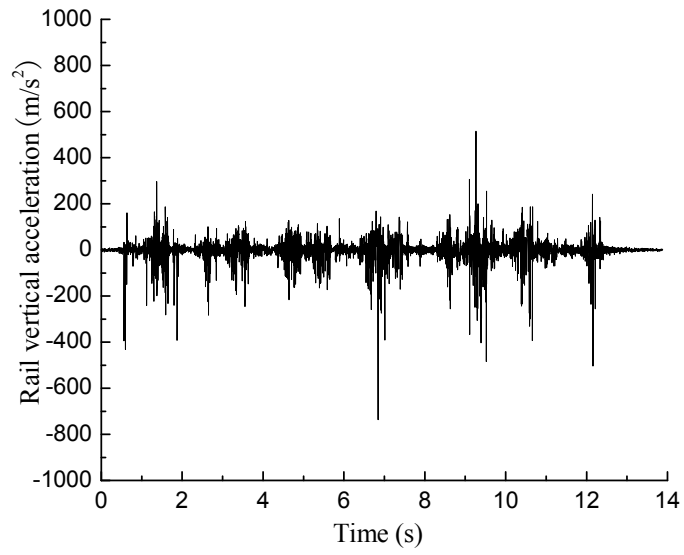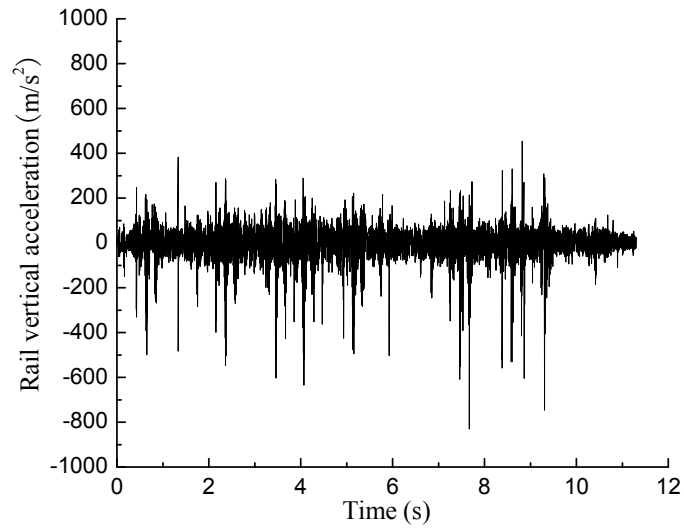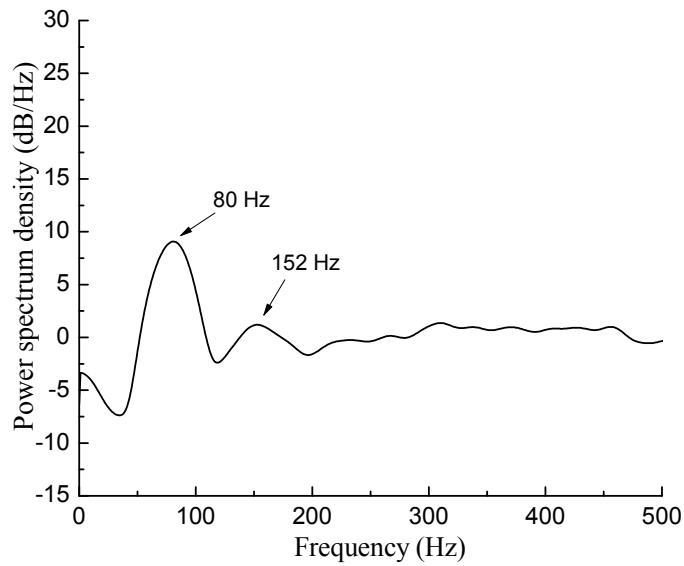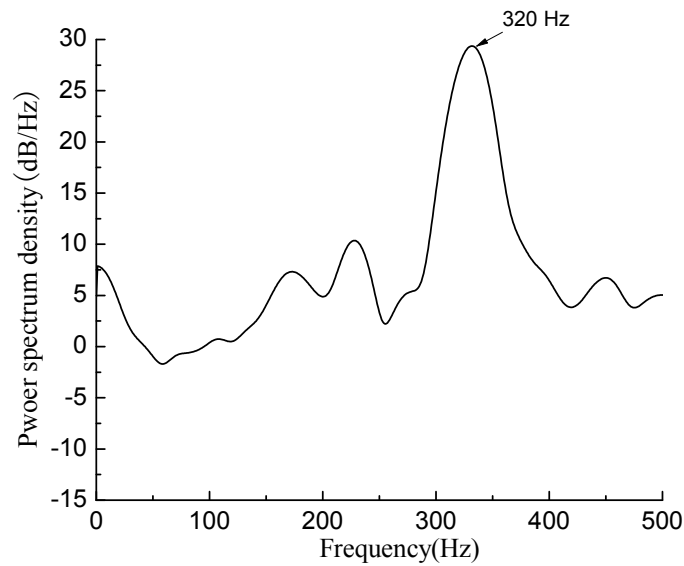
(a)
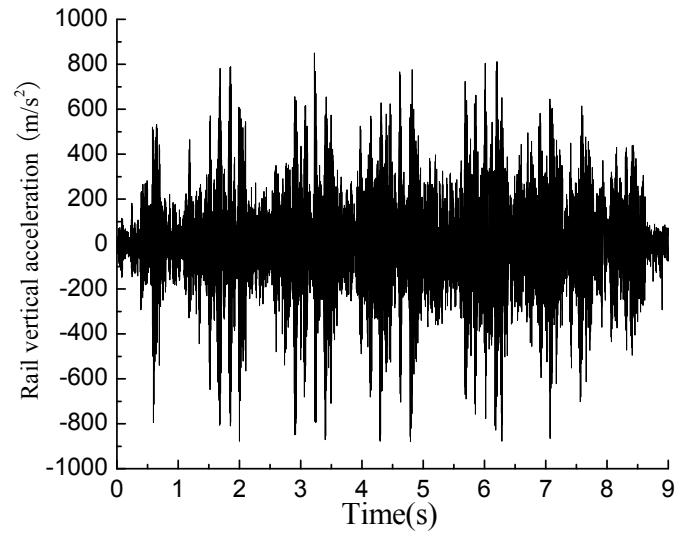
(b)
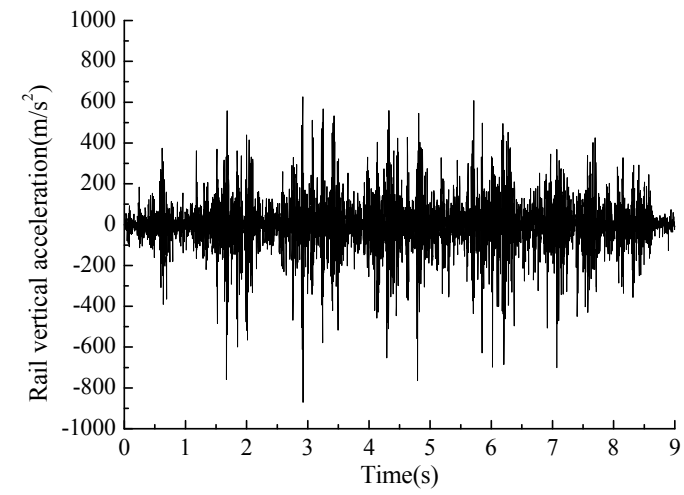
(c)

(d)

Figure 7 *Time history recorders of rail vibrations; measurement points were located at the rail center between two sleepers: (a) low rail at test site 1 with train speed 41.2 km/h, (b) left rail at test site 2 with train speed 48.9 km/h, (c) right rail at test site 2, and (d) low rail at test site 3, train speed 44.3 km/h.*
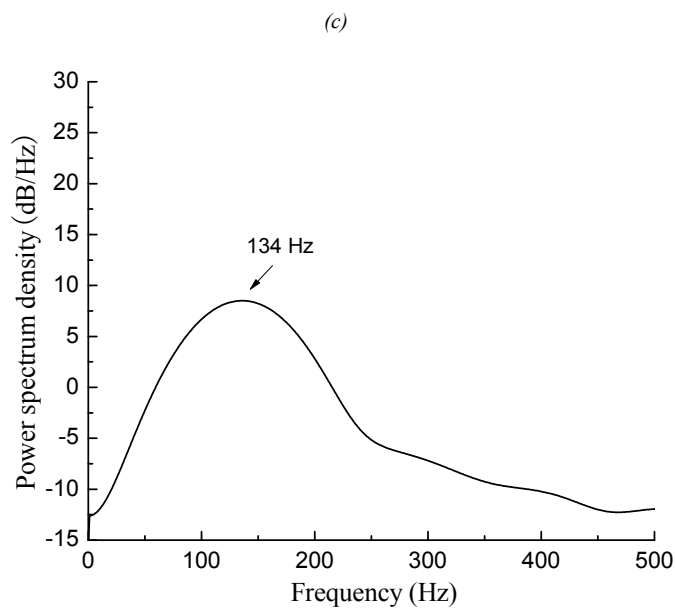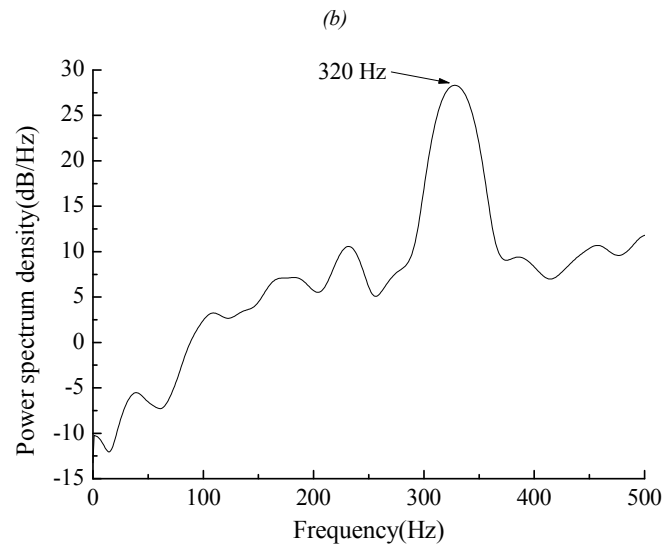

(a)

(d)

Figure 8 *PSD analysis of rail vibrations: PSD of vibration shown in (a) Figure 7(a), (b) Figure 7(b), (c) Figure 7(c), and (d) Figure 7(d).*

4.3. Rail corrugation prediction results

Figures 9–11 show three prediction results obtained by using the models shown in Figures 3–5. From Figure 9(a), it is seen that the two lowest frequencies of the self-excited vibration of the wheelset-track system at test site 1 are approximately 35.17 and 102.28 Hz. The mode shape corresponding to 102.28 Hz is shown in Figure 9(b). From the mode shape, it is seen that only the low rail and corresponding wheel are subjected to self-excited vibration. This suggests that only the low rail is subjected to rail corrugation. It must be mentioned that it is generally accepted in the brake squeal research community that the smaller the effective damping ratio, the more easily the corresponding unstable vibration occurs. However, some research has also shown that not only can the squeal corresponding to the smallest effective damping ratio occur, but sometimes the squeal corresponding to a larger negative effective damping ratio can also occur [36]. From Figure 10(a), it is seen that the miminum effective damping ratio corresponds to a self-excited vibration of frequency 291.76 Hz. The corresponding mode shape is shown in Figures 10(b) and 10(c). From the mode shape, it is seen that two rails and two wheels are subjected to self-excited vibrations. This suggests that the left and right rails are subjected to rail corrugation in that case. From Figure 11(a), it is seen that the miminum two frequencies of the

self-excited vibration of the wheelset-track system arre approximately 33.42 and 136.43 Hz. The mode shape corresponding to 136.43 Hz is shown in Figure 11(b). From the mode shape, it is seen that only the low rail and corresponding wheel are subjected to self-excited vibration. This suggests that only the low rail suffers from rail corrugation in that case.
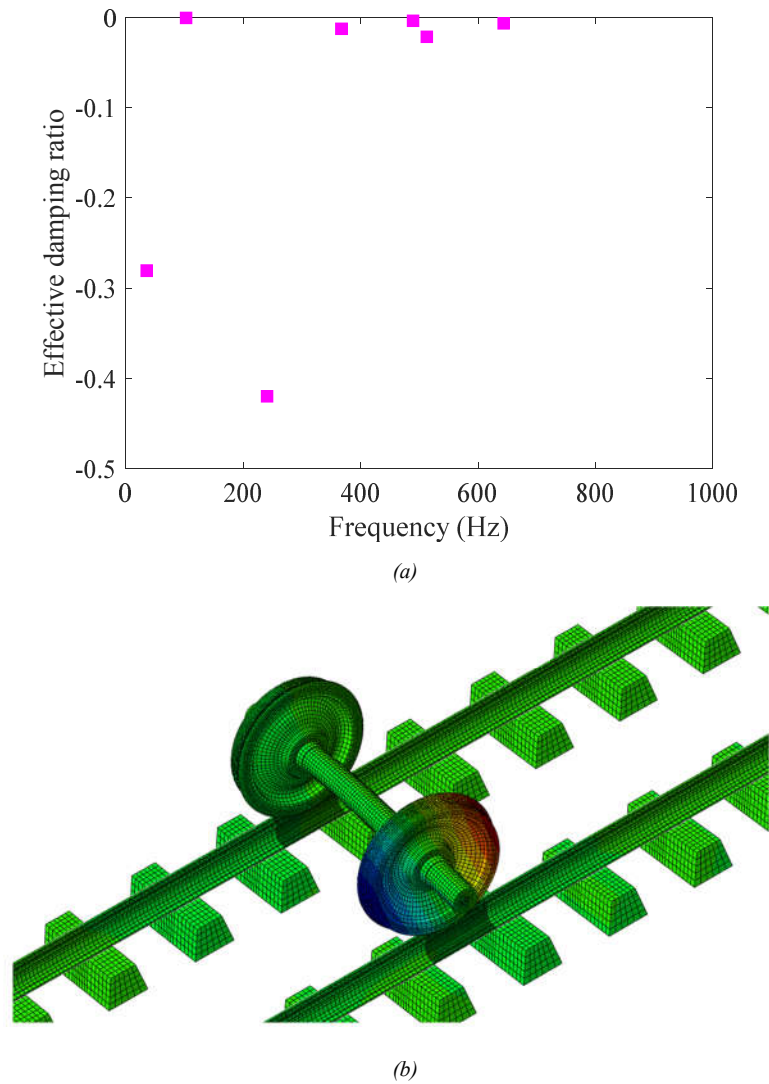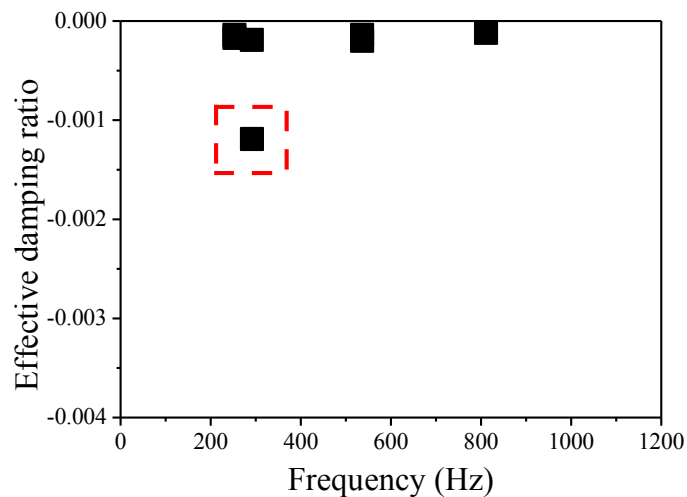

(a)

(b)

Figure 9 *Prediction result of rail corrugation in wheelset-track system shown in Figure 2(a): (a) frequency distribution of self-excited vibration of wheelset-track system; (b) mode shape of self-excited vibration of frequency f=102.28 Hz.*
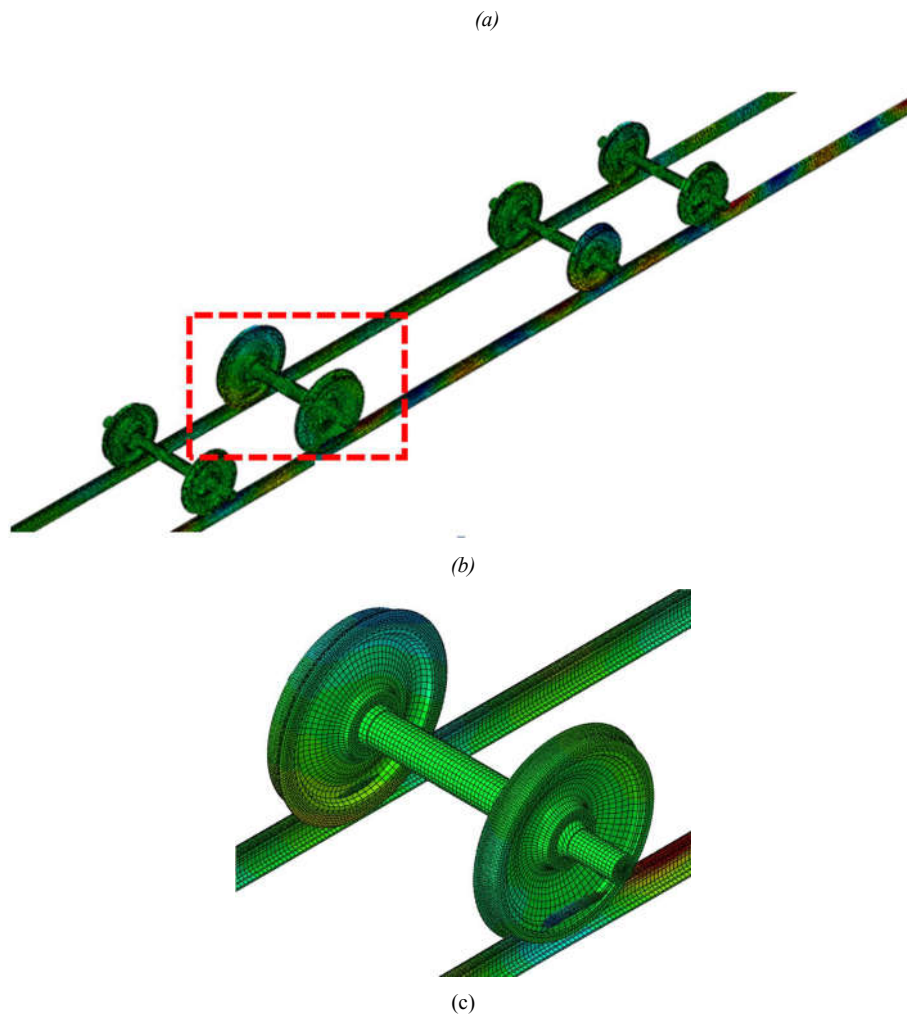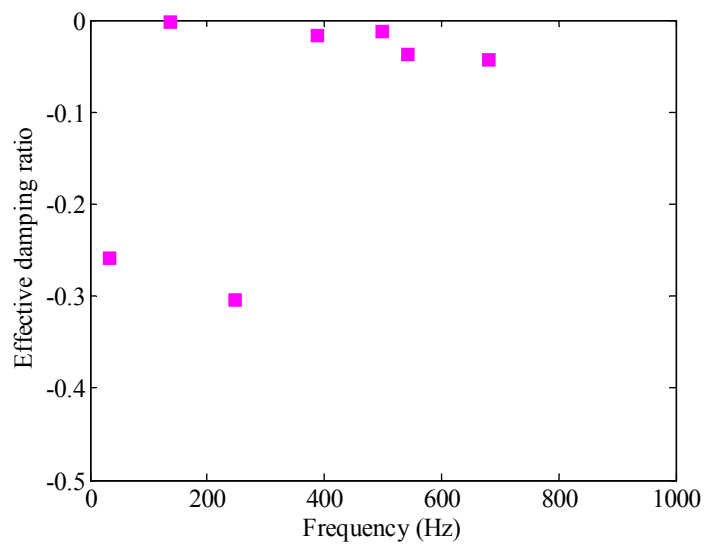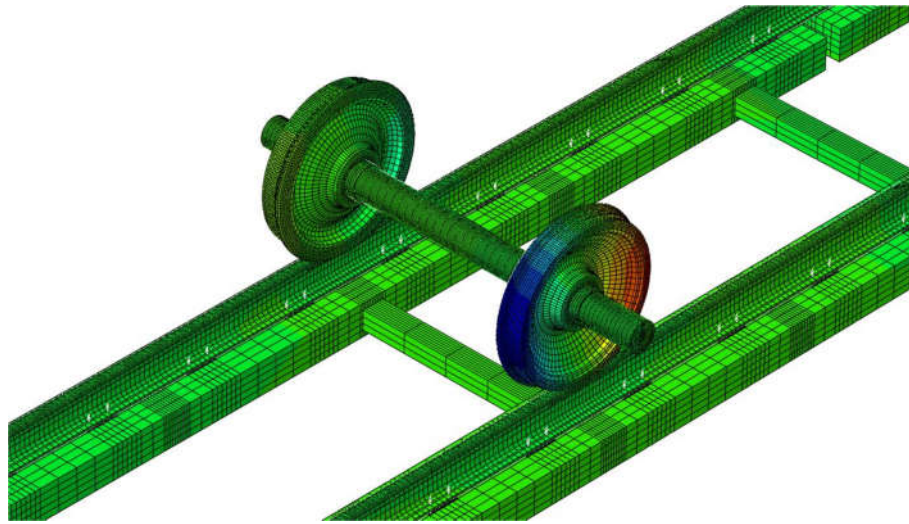
Figure 10 *Prediction result of rail corrugation in wheelset-track system shown in Figures 2(b) and 2(c): (a) frequency distribution of self-excited vibration of wheelset-track system; (b) mode shape of self-excited vibration of frequency 291.76 Hz; (c) details of mode shape of self-excited vibration of frequency 291.76 Hz.*

(b)

Figure 11 *Prediction result of rail corrugation in wheelset-track system shown in Figure 2(d): (a) frequency distribution of self-excited vibration of wheelset-track system; (b) mode shape of self-excited vibration of frequency 136.43 Hz.*

5. Discussion

Several researchers have reported that they validated their models [20,21,25,34], making significant progress in the study of rail corrugation. However, under close examination, it can be found that many rail corrugation prediction models in the literature do not take the effect of the radius of curved tracks into account. Rail corrugation is always predicted using these models when the necessary model parameters, except the radius of the curved track, are input to the models, whether the track is a tight curved or smooth curved one. In fact, two rails on a smooth curved or tangential track are rarely subjected to corrugation according to the CD phenomenon of rail corrugation. Obviously, the prediction results are not consistent with the CD phenomenon of rail corrugation.

The authors think that the reason that it is difficult to satisfactorily reproduce the CD phenomenon of rail corrugation with some models in the literature may be attributed to a flaw in the validation methods of their rail corrugation models. The authors think that in the validation method the identification of the generation mechanism of the rail vibration that can lead to rail corrugation has been neglected; that is to say, the vibration evolution with time before corrugation occurs has been neglected. Chen, one of the authors of the present paper, and collaborators studied the rail vibration evolution before rail corrugation occurred [37], and found that there were several types of rail vibrations with different frequencies before rail corrugation occurred, and that not all these vibrations could lead to rail corrugation. These several types of vibrations were considered to be excited by the rail surface roughness or friction coupling. Then, the authors also measured vibrations of two rails on a main-line tangential track when trains passed through and found that there were always some vibrations in these two rails when trains passed through, but these vibrations could not cause rail corrugation because the two rails have not suffered from corrugation in the previous decade. After serious consideration, the authors believe that the rail surface roughness measured in step 1 in the validation method is not the necessary and sufficient condition for rail corrugation to emerge. This is because random roughness has also led to rail corrugation. According to the CD phenomenon of rail corrugation, if a new rail is laid as the low rail of a tight curved track, the probability of the rail suffering from corrugation is close to 100%. If the new rail is laid as a rail of a tangential track, however, the probability of the rail suffering from corrugation is smaller than 5%–10%. This fact supports the conclusion that the rail surface roughness is not the necessary and sufficient condition for rail corrugation generation.

The CD phenomenon of rail corrugation is observed all over the world. Therefore, the authors propose using the CD phenomenon of rail corrugation as a global benchmark condition for the validation of rail corrugation models. If the prediction result of a model is consistent with the CD phenomenon of rail corrugation, the rail corrugation model is considered to be validated.

In the present field tests, the measured corrugation frequencies are 80 Hz for the wheelset-track system shown in Figure 2(a), 320 Hz for the wheelset-track system shown in Figures 2(b) and 2(c), and 134 Hz for the wheelset-track system shown in Figure 2(d). In the prediction of rail corrugation, the predicted corrugation frequencies are 102.28 Hz for the wheelset-track system shown in Figure 2(a), 291.76 Hz for the wheelset-track system shown in Figures 2(b) and 2(c), and 136.43 Hz for the wheelset-track system shown in Figure 2(d). The relative errors are 27.85%, 8.83%, and 1.81%, respectively. It is noted that the relative error of 27.85% seems too large. In planned follow-up work, the authors aim to make several improvements in the model to increase the low-frequency accuracy. The models can predict that the low rail of the tight curved track suffers from corrugation, but the high rail does not. The models can also predict that rail corrugation rarely occurs on smooth curved and tangential tracks. This is because the creep forces are not saturated in these cases; therefore, friction-induced self-excited vibration of the wheelset-track systems does not occur. Hence, one can see that the models established by the authors can predict the CD phenomenon of rail corrugation.

6. Conclusions

In this study, rail corrugation field measurement and prediction results are presented. A comparison between the field measurement and prediction results was performed and further discussion made. The following conclusions can be drawn:

1. Corrugation profiles of rails at three different sites were measured. Finite-element prediction models of these three corrugation profiles were established and analyzed. The relative errors between the rail corrugation measurement results and prediction results are 27.85%, 8.83%, and 1.81%, respectively. The prediction results are consistent with the measurement results and CD phenomenon of rail corrugation. Therefore, the model established by the authors can be used to predict rail corrugation.
2. The authors proposed the CD phenomenon of rail corrugation as a benchmark condition for the validation of rail corrugation models. If the prediction result of a model is consistent with the CD phenomenon of rail corrugation, the rail corrugation model is considered to be validated.

ORCID iD

GX Chen iD http://orcid.org/0000-0003-2552-4655

References

[1] Grassie SL, Kalousek J. Rail corrugation: characteristics, causes and treatments. Proceedings of the Institution of Mechanical Engineers, Part F: Journal of Rail and Rapid Transit, 1993, 207(1) 57-68.

[2] Grassie SL. Rail corrugation: characteristics, causes, and treatments. Proceedings of the Institution of Mechanical Engineers, Part F: Journal of Rail and Rapid Transit, 2009, 223(6): 581-96.

[3] Sato Y, Matsumoto A, Knothe K. Review on rail corrugation studies. Wear, 2002, 253(1-2) 130-139.

[4] Oostermeijer KH. Review on short pitch rail corrugation studies. Wear, 2008, 265(9-10) 1231-1237.

[5] Kalousek J, Johnson K. An investigation of short pitch wheel and rail corrugations on the Vancouver mass transit system. Proceedings of the Institution of Mechanical Engineers, Part F: Journal of Rail and Rapid Transit, 1992, 206(2) 127-135.

[6] Nielsen JCO, Lund NR, Johansson A, et al. Train-track interaction and mechanisms of irregular wear on wheel and rail surfaces. Vehicle System Dynamics, 2003, 40(1-3) 43-54.

[7] Gomez J, Vadillo EG, Santamaria J. A comprehensive track model for the improvement of corrugation models. Journal of Sound and Vibration, 2006, 293(3) 522-534.

[8] Valdivia AR. A linear dynamic wear model to explain the initiating mechanism of corrugation. Vehicle System Dynamics, 1988, 17(sup1) 493-496.

[9] Tassilly E, Vincent N. A linear model for the corrugation of rails. Journal of Sound and Vibration, 1991, 150(1) 25-45.

[10] Hempelmann K, Knothe K. An extended linear model for the prediction of short pitch corrugation. Wear, 1996, 191(1) 161-169.

[11] Muller S. A linear wheel-rail model to investigate stability and corrugation on straight track. Wear, 2000, 243(1) 122-132.

[12] Igeland A, Ilias H. Rail head corrugation growth predictions based on non-linear high frequency vehicle/track interaction. Wear, 1997, 213(1) 90-97.

[13] Torstensson PT, Nielsen JCO. Simulation of dynamic vehicle-track interaction on small radius curves. Vehicle System Dynamics, 2011, 49(11) 1711-1732.

[14] Meehan PA, Daniel WJT, Campey T. Prediction of the growth of wear-type rail corrugation. Wear, 2005, 258(7-8) 1001-1013.

[15] Sheng X, Thompson DJ, Jones CJC, et al. Simulations of roughness initiation and growth on railway rails. Journal of Sound and Vibration, 2006, 293(3-5) 819-829.

[16] Brockley CA, Ko PL. An investigation of rail corrugation using friction-induced vibration theory. Wear, 1988, 128(1) 99-105.

[17] Suda Y, Hanawa M, Okumura M, et al. Study on rail corrugation in sharp curves of commuter line. Wear, 2002, 253(1) 193-198.

[18] Wu TX, Thompson DJ. An investigation into rail corrugation due to micro-slip under multiple wheel/rail interactions. Wear, 2005, 258(7-8) 1115-1125.

[19] Sun YQ, Simson S. Wagon-track modelling and parametric study on rail corrugation initiation due to wheel stick-slip process on curved track. Wear, 2008, 265(9-10) 1193-1201.

[20] Torstensson PT, Schilke M. Rail corrugation growth on small radius curves-Measurements and validation of a numerical prediction model. Wear, 2013, 303(1-2) 381-396.

[21] Hiensch M, Nielsen JCO, Verheijen E. Rail corrugation in The Netherlands-measurements and simulations. Wear, 2002, 253(1-2) 140-149.

[22] Tassilly E, Vincent N. Rail corrugations: analytical model and field tests. Wear, 1991, 144(1-2) 163-178.

[23] Diana G, Cheli F, Bruni S, et al. Experimental and numerical investigation on subway short pitch corrugation. Vehicle System Dynamics, 1998, 29(S1) 234-245.

[24] Batten RD, Bellette PA, Meehan PA, et al. Field and theoretical investigation of the mechanism of corrugation wavelength fixation under speed variation. Wear, 2011, 271(1-2) 278-286.

[25] Bellette PA, Meehan PA, Daniel WJT. Validation of a tangent track corrugation model with a two disk test rig. Wear, 2011, 271(1-2) 268-277.

[26] Vila P, Fayos J, Baeza L. Simulation of the evolution of rail corrugation using a rotating flexible wheelset model. Vehicle System Dynamics, 2011, 49(11) 1749-1769.

[27] Baeza L, Vila P, Xie G, et al. Prediction of rail corrugation using a rotating flexible wheelset coupled with a flexible track model and a non-Hertzian/non-steady contact model. Journal of Sound and Vibration, 2011, 330(18-19) 4493-4507.

[28] Jin XS, Wen ZF, Wang KY, et al. Three- dimensional train-track model for study of rail corrugation. Journal of Sound and Vibration, 2006, 293(3-5) 830-855.

[29] Bellette PA, Meehan PA, Daniel WJT. Contact induced wear filtering and its influence on corrugation growth. Wear, 268 (2010) 1320-1328.

[30] Chen GX, Zhou ZR, Ouyang H, et al. A finite element study on rail corrugation based on saturated creep force-induced self-excited vibration of a wheelset–track System. Journal of Sound and Vibration, 2010, 329: 4643-4655.

[31] Cui XL, Chen GX, Yang HG, et al. Effect of the wheel/rail contact angle and the direction of the saturated creep force on rail corrugation. Wear, 2015, 330: 554-562.

[32] Cui XL, Chen GX, Yang HJ, et al. A case study of rail corrugation phenomenon based on the viewpoint of friction-induced oscillation of a wheelset-track system. Journal of Vibroengineering, 2017, 19(6) 4516-4530.

[33] Omar El Beshbichi. Complex Eigenvalue Analysis (CEA) and Design of Experiment Analysis(DOE) towards the investigation of the interaction effects of track components on rail corrugation development. MS Dissertation, Italy, Politecnico di Milano, 2017.11

[34] Correa N, Vadillo E, Santamria J, et al. A versatile method in the space domain to study short-wave rail undulatory wear caused by rail surface defects. Wear, 2016, 352(1) 196-208.

[35] Oregui M, Li Z, Dollevoet R. An investigation into the modeling of railway fastening. International Journal of Mechanical Sciences, 2015, 92: 1-11.

[36] Kung SW, Stelzer G, Belsky V, et al. Brake squeal analysis incorporating contact conditions and other nonlinear effects. SAE technical paper series, 2003-01-3343.

[37] Chen GX, Wu YF, Cui XL, et al. Study on the vibration causing rail corrugation. The Proceedings of 25th International Symposium on Dynamics of Vehicles on Roads and Tracks, 2017, Rockhampton, Queensland, Australia.